High-sensitivity Polarization-independent Biochemical Sensor based on Silicon-on-insulator Cross-slot Waveguide

Chao Pan and B. M. A. Rahman, *Fellow, IEEE*

***Abstract*—Slot waveguides reported so far are strongly polarization dependent. The concept of a novel cross-slot waveguide (WG) is presented here, which contains both vertical and horizontal slots and supports the power enhancement in the slot region for both the quasi-TE and quasi-TM polarizations. This WG can be fabricated by exploiting well developed CMOS technology. For the unpolarized operating light, the cross-slot WG is optimized to have the maximum total slot confinement factors for the two polarizations. As for a polarization-independent design, confinement in slot for each polarization can reach 39.4% when the silicon core width and height are set to around 223 nm and 216 nm, respectively. It is shown here that a biochemical sensor employing a cross-slot-WG exhibits a significantly better sensitivity, compared to either a vertical-slot-WG or a horizontal-slot-WG based biochemical sensor. As an example, when both the vertical slot width and horizontal slot height are set to 100 nm, its sensitivity is almost double compared with a simple vertical or horizontal slot with 100 nm gap.**

***Index Terms*—Silicon photonics, cross-slot waveguide, biochemical sensing, polarization independent, high sensitivity, finite element analysis.**

I. Introduction

In recent years, there has been a gradual increase of research interest for silicon photonic technology [1] based on silicon-on-insulator (SOI) platform. It has the potential to reduce power consumption, size, and cost; and it can also increase the functionality and reliability of a Photonic Integrated Circuit (PIC). For SOI technology, PICs fabricated on silicon (Si) substrate can take the advantage of mature CMOS technology to develop and create high performance lap-on-a-chip micro-systems combining both photonics and electronics on the same chip, applied in chemical and biochemical analysis [2], which is very attractive nowadays.

In this framework, optical sensing by SOI-waveguide (WG)-based devices has gained more attention. In an optical SOI WG sensor for chemical and biochemical analysis, its effective index is affected either by the change of the refractive index of the cladding medium, known as homogeneous sensing, or the change in the thickness of an ultra-thin layer of receptor molecules which are immobilized on WG surface, known as surface sensing [3]. Based on that, various kinds of integrated optical structures have been proposed to measure the change in the effective index, such as those based on directional couplers [4], Mach-Zehnder interferometers [5], and micro ring resonators [6].

For most of the optical WGs, light is confined in the core due to higher index there. Therefore, light interaction with the sensing material in the cladding region or at the surface of the nanowire is limited, leading to the low sensitivity of these devices. However, the unique feature of a slot WG [7], where light is guided in a low index region allows easy access of the sensing layer to high field region. Thus, apparently, the enhancement of light interaction in the sensing region can improve sensitivity of the sensor. The guidance property in a slot WG is due to the continuity of the normal component of the Electric Flux Density, D_n, which increases the normal component of the Electric Field, E_n, in the low index region. There are two possible types of slot WGs, relating to their structural orientation, called the vertical and horizontal slot WGs. In a vertical slot, E_x field is enhanced, which is the dominant component for the quasi-TE mode and normal to the vertical interfaces. Similarly, for a horizontal slot, the dominant E_y component of the quasi-TM mode increases inside the slot due to the continuity condition of the D_y at the interfaces. However, as stated above, unfortunately both the horizontal and vertical slot guides confine only one specific polarization.

Currently, research work on the employment of vertical or horizontal slot WG as a biochemical sensor has been proposed in [8] [9]. For the first time, in this work it is being reported here that by combining a vertical and a horizontal slots it is possible to design and optimize an SOI cross-slot WG for biochemical sensing which can support simultaneously both the polarized waves. As a high index contrast necessary to enhance the power in the slot region, the optical mode in such a waveguide is hybrid in nature, so, a full-vectorial numerical method is needed to characterize biochemical sensor based on such a structure and in this work, a rigorous full-vectorial **H**-field based finite element formulation [10] is used here to optimize such sensors to achieve a polarization-independent design. Their sensitivity is also found to be significantly larger,

This paragraph of the first footnote will contain the date on which you submitted your paper for review.

Chao Pan is with the School of Electronic Science & Engineering, Southeast University, Nanjing, Jiangsu Province, 210096 P. R. China (e-mail: p.c.1987@163.com).

B. M. A. Rahman is with the School of Engineering and Mathematical Sciences, City University London, London, EV1V 0HB, U.K. (e-mail: b.m.a.rahman@city.ac.uk).

compared with that of a sensor based on either vertical or horizontal slot WGs with similar dimensions.

II. Theory

Optical biochemical sensing such as DNA sequencing by hybridization, antigen-antibody reactions study or pollution concentration measurement in water are mainly based on immobilization of an ultra-thin layer of receptor molecules on the WG surface. Effective index, n_{eff} of the guided mode in a WG is affected by the change of molecular adlayer (which can be called sensing layer) thickness caused by the interaction between analyte and receptor molecules. The WG sensitivity, S, can be defined as [3]:

$$S = \frac{\partial n_{eff}}{\partial \tau} \tag{1}$$

where τ is the thickness of the sensing layer.

The change in n_{eff}, Δn_{eff}, produced by the change of the sensing layer thickness, $\Delta\tau$, can be related approximately by the light confined in sensing layer and there is a positive correlation between the Δn_{eff} and confinement factor in the sensing layer for the guided modes in a slot WG [3], which can be defined as:

$$\Gamma_S = \frac{\iint_S \mathrm{R_e}(\mathbf{E}\times\mathbf{H}^*)dxdy}{\iint_\infty \mathrm{R_e}(\mathbf{E}\times\mathbf{H}^*)dxdy} \tag{2}$$

where **E** is the electric field, **H** is the magnetic field, * denotes a complex conjugate, R_e returns the real part of a complex number, and S indicates sensing layer.

Similarly, confinement factor in the slot region of a slot WG can also be defined as:

$$\Gamma_G = \frac{\iint_G \mathrm{R_e}(\mathbf{E}\times\mathbf{H}^*)dxdy}{\iint_\infty \mathrm{R_e}(\mathbf{E}\times\mathbf{H}^*)dxdy} \tag{3}$$

where G indicates slot region.

To achieve an accurate design, a rigorous numerical approach is needed to calculate the confinement factors, together with the change in the guided mode effective index by sensing. As to all practical optical WG with 2D confinement, the eigenmodes are classified as quasi-TE and quasi-TM modes, and they contain all the six components of the **E** and **H** fields. Thus, a full-vectorial numerical method should be used to find accurate eigenmodes in these WGs.

The full-vectorial numerical method used here is an **H**-field based FEM, one of the most accurate and numerically efficient approaches. This formulation is based on the minimization of the full **H**-field energy functional [10],

$$\omega^2 = \frac{\iint[(\nabla\times\boldsymbol{H})^*\cdot\hat{\varepsilon}^{-1}(\nabla\times\boldsymbol{H}) + p(\nabla\cdot\boldsymbol{H})^*(\nabla\cdot\boldsymbol{H})]dxdy}{\iint \boldsymbol{H}^*\cdot\hat{\mu}\boldsymbol{H}dxdy} \tag{4}$$

where ω^2 is the eigenvalue (ω being the angular frequency), p is a weighting factor for penalty term to eliminate spurious modes and $\hat{\varepsilon}$ and $\hat{\mu}$ are permittivity and permeability tensors, respectively.

III. Results and Discussion

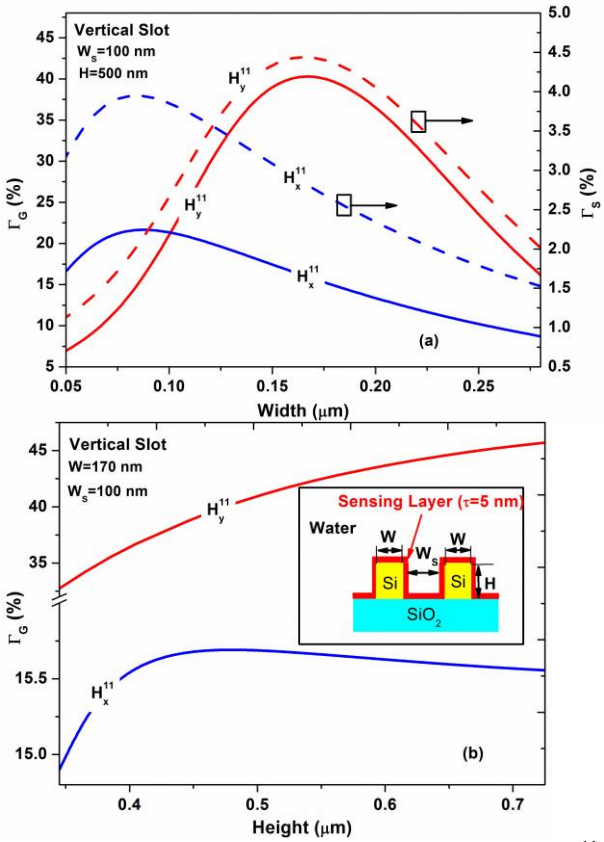

Fig. 1. Variations of Γ_G and Γ_S for the fundamental quasi-TE, H_y^{11} and quasi-TM, H_x^{11} modes with the (a) width, W and (b) height, H of the silicon core.

First, biochemical sensors based on vertical and horizontal slot WGs are characterized. The structure of a typical vertical slot WG for biochemical sensing [6] is shown as an inset in Fig. 1 (b). The WG is completely covered with a thin sensing layer with a refractive index value of 1.45. Refractive indices of silicon core, SiO_2 substrate, and the aqueous solution are taken as 3.47548, 1.44402, and 1.33, respectively. Initially, the sensing layer thickness, τ and the slot width, W_S are taken as 5 nm and 100 nm, respectively. Variations of Γ_G and Γ_S for the fundamental quasi-TE mode, H_y^{11}, with the width of the silicon core are shown in Fig. 1 (a) by red solid and dashed lines, respectively, while those for the fundamental quasi-TM mode, H_x^{11}, are shown by blue solid and dashed lines, respectively. It can be observed that variations of Γ_G and Γ_S for both the polarizations with the silicon core width have similar tendencies, and it indicates that either Γ_G or Γ_S can be used as an optimization parameter when optimizing the dimensions of the silicon cores in a slot WG. For this work, in optimizing the dimension of the silicon cores, Γ_G is taken as the optimization parameter. These results can also be used as a reference for the design of the slot WG for homogeneous sensing. It can also be observed that confinement factors in the slot region, Γ_G for both the polarizations increase at first and then decrease with the increase of the silicon core width, but they have their peaks at different values of the width. The Γ_G for the H_y^{11} mode reach its maximum value of 40.7% when the width is 160 nm, while Γ_G for the H_x^{11} mode reach its maximum value of only 21.9% when

the width is 80 nm. Obviously, as for a vertical slot, the dominant E_x field of the H_y^{11} mode is enhanced in the slot region, and thus the maximum value of Γ_G for the H_y^{11} mode is nearly double than that for the H_x^{11} mode. It should be noted that although the difference between the maximum values of Γ_S for the H_y^{11} and H_x^{11} modes is about 0.5%, the coupling loss for the H_x^{11} mode input in a vertical slot WG, whose field is bimodal, is very large due to the large spot mismatching between the WG and the laser whose mode field is generally unimodal. As a result, in a vertical slot WG, quasi-TE mode should be employed as the operating polarization. Variations of Γ_G for the H_y^{11} and H_x^{11} modes with the silicon core height, H of a vertical slot WG are shown in Fig.1 (b) by red and blue lines, respectively. Widths of the silicon core and slot are taken as 160 nm and 100 nm, respectively. It is shown here that with the increase in height, Γ_G for the H_y^{11} mode increases monotonically but slows down at a larger height. On the other hand, Γ_G for the H_x^{11} mode increases at first and decreases slightly after reaching the highest value but this is much smaller.

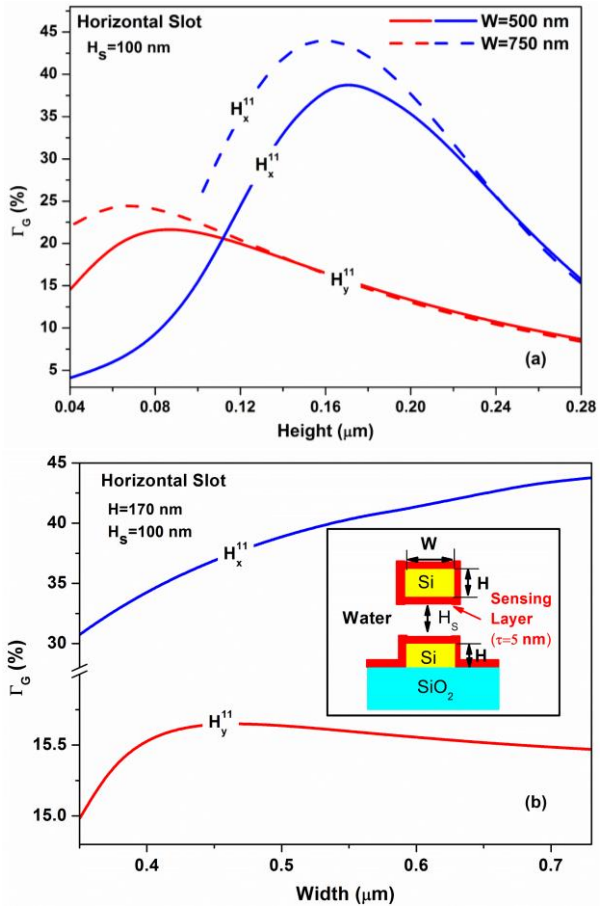

Fig. 2. Variations of Γ_G for the H_y^{11} and H_x^{11} modes with the dimension of silicon cores: (a) with the silicon core height, H for the different silicon core widths, (b) with the silicon core width, W when their height is set to 170 nm.

Next, optimization of a horizontal slot waveguide for biochemical sensing (shown as an inset in Fig. 2 (b)) is carried out. The horizontal slot WG with aqueous solution or air in the slot region, which is designed to be connected with tapered and feed WGs, can be fabricated by controlling the etching process [9]. Here, the horizontal slot height is taken as 100 nm. Variations of Γ_G for the H_y^{11} and H_x^{11} modes with the silicon core height, H, for W=500 nm are shown in Fig. 2 (a) by solid red and blue lines, respectively, while those for W=750 nm, are shown by dashed red and blue lines, respectively. It can be observed that Γ_G for the H_x^{11} mode increases at first, reaches its maximum value of 38.9% when H = 170 nm and then decreases with the further increase of silicon core height. The maximum value of Γ_G for the H_x^{11} mode is significantly bigger than that for the H_y^{11} mode, as the dominant E_y field of H_x^{11} mode is enhanced in the horizontal slot region. It can also be observed that when the width is increased from 500 nm to 750 nm, for the H_x^{11} mode can reach its peak value, up to 44.6%, but at a slightly lower height, H = 160 nm. Variations of Γ_G for the H_y^{11} and H_x^{11} modes with the silicon core width, W of a horizontal slot WG whose height is set to 170 nm, are also shown in Fig.2 (b). Their tendencies are similar to those of Γ_G for the H_y^{11} mode in a vertical slot WG but with the silicon core height. Overall, it is true that there is a strong correspondence between the vertical and horizontal slot WGs, and the variation characteristics of Γ_G for the H_y^{11} and H_x^{11} modes with the silicon core width and height for a vertical slot WG are nearly similar as the variation characteristics of Γ_G for the H_x^{11} and H_y^{11} modes with the silicon core height and width for a horizontal slot WG, respectively.

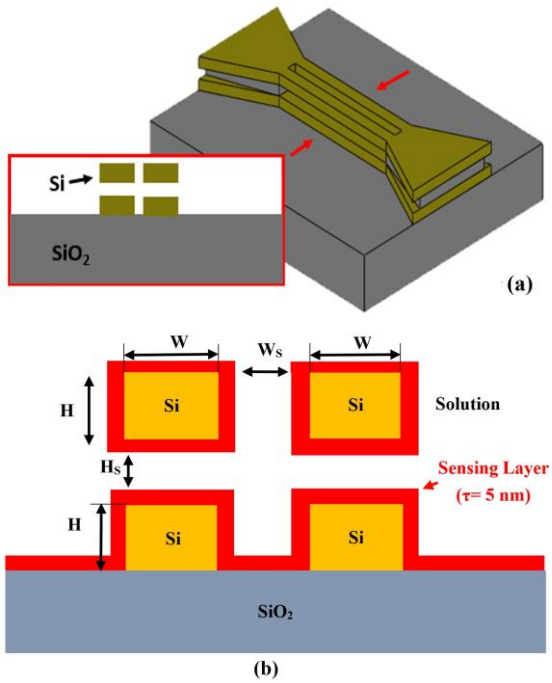

Fig. 3. (a) Schematic diagram of cross-slot waveguide with hollow vertical and horizontal slots. (b) Diagram of a cross-slot waveguide for biochemical sensing.

In this section, a novel cross-slot WG for biochemical sensing which supports field enhancement in the slot region for both quasi-TE and quasi-TM modes is proposed. The cross-slot WG is composed of both vertical and horizontal slot regions, as shown in Fig. 3 (a). This structure can be designed to connect via the tapered WGs and can be fabricated on a SOI wafer with

a 220-nm top-Si layer (or a thicker layer if necessary) on a 2 μm or similar thick buried oxide (BOX) layer. If necessary, the top waveguiding silicon layer can be thinned down to an optimized thickness. On top of this, SiO_2 can be deposited through plasma enhanced chemical vapor deposition (PECVD) [11]. Following that a low-loss hydrogenated amorphous silicon (a-Si) layer can be deposited followed by a thin SiO_2 layer deposition, which can act as a hard mask, by using PECVD [11]. If necessary these layers can be planarized by using chemical mechanical polishing (CMP), before the next layer deposition. A vertical slot waveguide can be defined by Deep UV (DUV) or E-beam lithography and followed by dry etching of silicon and SiO_2 layer down to the BOX layer. Next, buffered hydrofluoric acid can be used to etch the SiO_2 layer in between the two horizontal silicon guiding layers to form the horizontal slot [12][13]. Since width of the two horizontal slots in between two silicon layers is smaller, hydrofluoric acid introduced through the vertical slot and outside will remove this SiO_2 layer earlier than the much wider SiO_2 layer beyond the vertical slot channel. Once the low-index oxide layer under the narrow waveguide region is removed then the etching process is stopped so that two upper silicon layers are mechanically supported by the wider region at the two ends where silica was only partially removed. However, it should be noted that any CMOS compatible material, such as Si_3N_4 [14], can also be used to fabricate the initial slot regions, which later on needs to be selectively removed to open up the empty slot region. Previously, sensing arm of several micron long incorporating cantilever suspension from one end has been fabricated with negligible deformation [15]. However, since for the proposed structure only a short length of slot waveguide is suspended from both the ends it is expected to be mechanically sturdier. After the cross-slot WG is formed, the several nm-thick sensing layer for biochemical sensing can be added to all the surface of the silicon cores [6], [13], [16], [17] such as silanized with 3-glycidyloxy propylitrimethoxy saline for label-free protein sensing [6], or dipped into aqueous glutaraldehyde for the study of label-free molecular binding reactions [17], as shown in Fig. 3 (b). Here the thickness of sensing layer is taken as 5 nm.

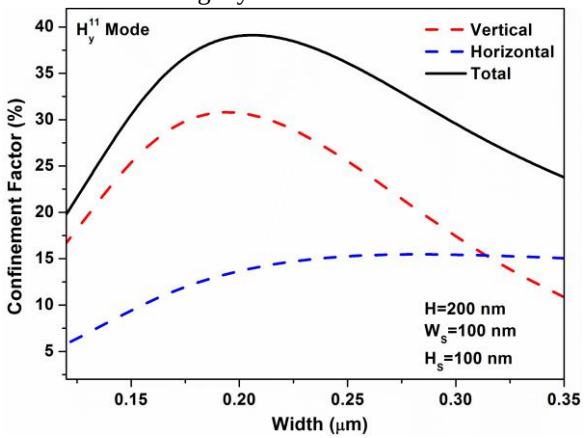

Fig. 4. Variations of confinement factors in the vertical, horizontal and total slot regions for the H_y^{11} mode with the width of silicon cores, W.

Variations of confinement factors in the vertical, horizontal and total slot regions for the H_y^{11} mode with the width of silicon cores, W are shown in Fig. 4. The silicon core height, H, the vertical slot width, W_S and the horizontal slot height, H_S are taken as 200 nm, 100 nm, and 100 nm, respectively. It can be observed that for the H_y^{11} mode, with the increase of the silicon core width, the confinement factor in the vertical slot region increases at first and then it decreases. Its maximum value is 29.7% when the silicon width is 190 nm. The confinement factor in the horizontal slot region also increases at the beginning but asymptotically reaches its stable value when the silicon core width increases. For quasi-TE mode, as its dominant E_x field is enhanced in the vertical region, which is shown in Fig. 5 (a), it's vertical confinement is dominant here. Therefore, maximum value of the confinement factor in the vertical slot region is much larger than that in the horizontal slot region. Variation of the confinement factor in the whole slot regions (total-slot confinement factor, Γ_{T-Hy}) with the silicon width has the similar tendency as the vertical slot, but reaches its maximum value of 39.4%, when W=210 nm. Correspondingly, for the H_x^{11} mode, the maximum value of the confinement factor in the vertical slot region is much lower than that in the horizontal slot region, for dominant E_y field of the quasi-TM mode (shown in Fig. 5 (b)) is enhanced in the horizontal region.

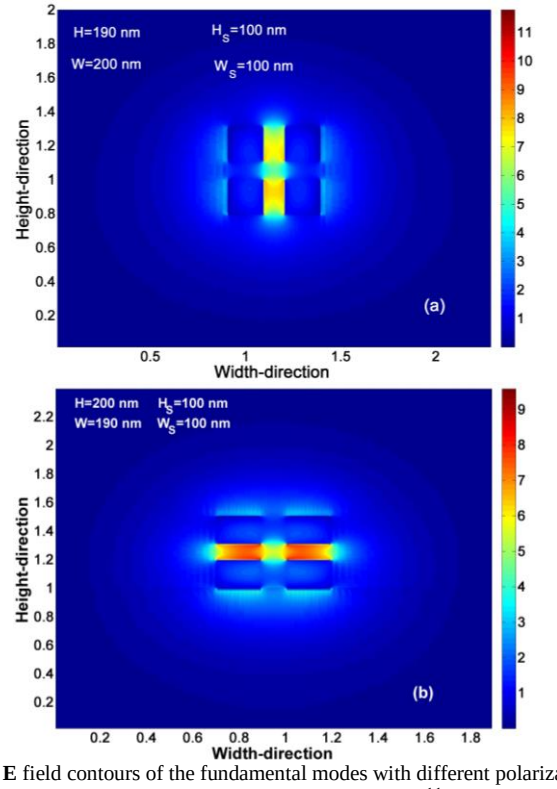

Fig. 5. **E** field contours of the fundamental modes with different polarizations in a cross-slot waveguide: (a) E_x field contour of the H_y^{11} mode, (b) E_y field contour of the H_x^{11} mode.

Variations of total-slot confinement factors for the H_y^{11} mode, Γ_{T-Hy}, with the width of silicon cores, W for different silicon core heights, H=100 nm, 200 nm, and 300 nm are shown in Fig. 6 (a) by green, blue, and red lines, respectively. It can be observed that for the H_y^{11} mode, in all the cases, total-slot confinement factors increase at first and then decrease with the increase of the silicon core width, and they reach their peak

values at width values of 290 nm, 210 nm, and 160 nm for H=100 nm, 200 nm, and 300 nm, respectively. It can be concluded that for the H_y^{11} mode, the value of the silicon width for the highest total-slot confinement factor decreases with the increase of the silicon core height. These curves also show that higher total confinement factor can be obtained by using larger height, H and smaller width, W. Figure 6 (b) shows variations of Γ_{T-Hy} with the silicon core height, H for different silicon widths (W=200 nm, 170 nm, and 150 nm). It can be observed that in all the cases, for the H_y^{11} mode, with the increase of the silicon core height, the total-slot confinement factors increase at first and then asymptotically reach their stable values.

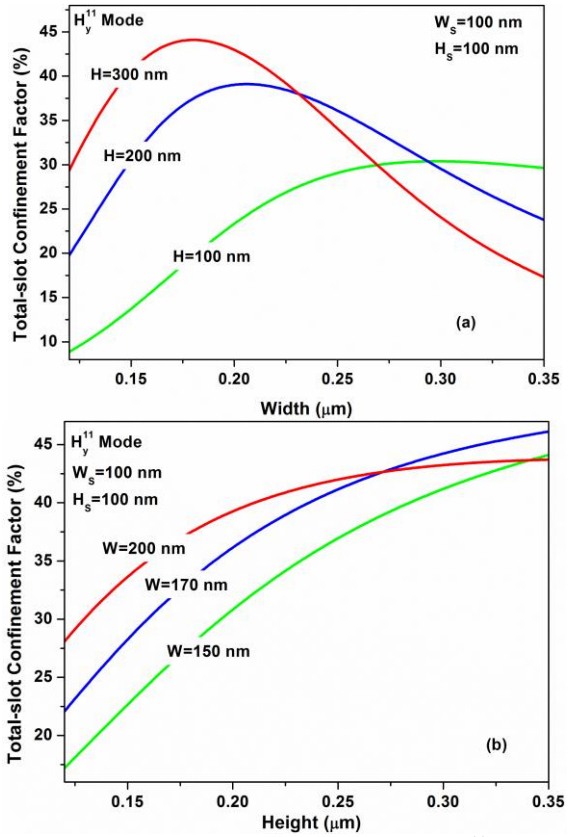

Fig. 6. Variations of total-slot confinement factors for the H_y^{11} mode with the silicon core (a) width and (b) height.

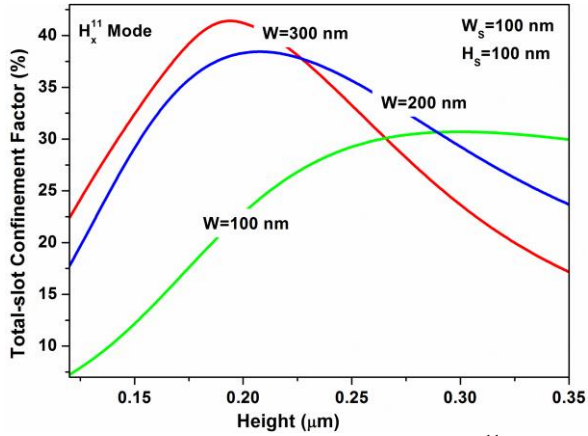

Fig. 7. Variations of total-slot confinement factors for the H_x^{11} mode with the silicon core height.

Variations of total-slot confinement factors for the H_x^{11} mode, Γ_{T-Hx}, with the height of silicon cores for different widths (W=100 nm, 200 nm, and 300 nm) are shown by green, blue, and red lines, respectively, in Fig. 7. It can be observed that in all the cases for the H_x^{11} mode, the total-slot confinement factors increase first and then decrease with the increase of the silicon core height. The value of silicon height for the highest total-slot confinement factor decreases with the increase in the silicon core height, similar to the variation of total-slot confinement factor with the silicon core width for the H_y^{11} mode. Variations of total-slot confinement factors for the H_x^{11} mode with the width of silicon cores also have the similar tendencies as those of the total-slot confinement factors for the H_y^{11} mode with the height of silicon cores, but not shown here. In order to make the comparison of the confinement factors in the total slot region between the cross and the vertical or horizontal slot WGs more reasonable, the height of the cross and vertical slot WGs should be set to the same value, or the width of the cross and horizontal slot WGs should be set to the same value. For the vertical or horizontal slot WG, the WG height or width equals to its silicon height or width. However, for the cross-slot WG, its WG width and height are taken as the summation of two silicon core and a vertical slot widths, and the summation of two silicon core and a horizontal slot heights, respectively. The maximum Γ_{T-Hy} in the slot region of the cross-slot WG is slightly less than that in the vertical slot WG, for instance, the maximum confinement factors are 39.4% and 40.9% in the slot regions of the cross and vertical slot WGs with the same WG height of 500 nm. Correspondingly, the maximum Γ_{T-Hx} in the slot region of the cross-slot WG nearly equals to that of the horizontal slot WG with the same WG width.

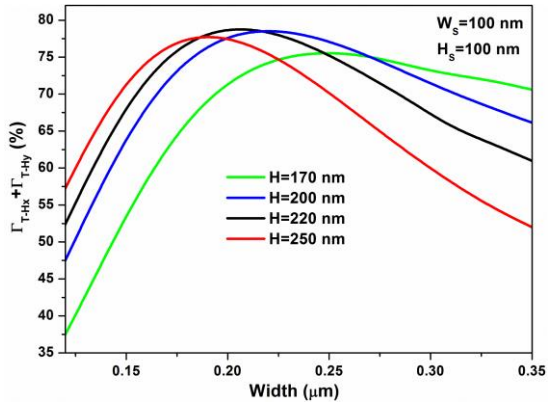

Fig. 8. Variations of $\Gamma_{T-Hy} + \Gamma_{T-Hx}$ with the width, W of silicon cores.

As shown in Fig. 6 (a), for the H_y^{11} mode, with increase in the silicon core height, the total-slot confinement factor may keep increasing by reducing the silicon core width continuously. Similarly, for the H_x^{11} mode, with the increase of the silicon core width, the total-slot confinement factor may keep increasing by reducing the silicon core height continuously. Next, summation of the total-slot confinement factors for the H_y^{11} and H_x^{11} modes, $\Gamma_{T-Hy} + \Gamma_{T-Hx}$ is taken as the optimization parameter to design a cross-slot WG with the highest sensitivity for its polarization independent operation. Variations of $\Gamma_{T-Hy} + \Gamma_{T-Hx}$ with the width, W of silicon

cores is shown in Fig. 8. It can be observed that for a given silicon core height (similar for width, but not shown here), with the increase of width, their summation increases at first and then decreases. It can also be observed when the width and height of the silicon cores are set to around 205 nm and 220 nm, respectively, the $\Gamma_{T-Hy} + \Gamma_{T-Hx}$ is as high as 79%, nearly the same as the summation of the maximum Γ_G for the H_y^{11} mode in the vertical slot WG with similar WG height and the maximum Γ_G for the H_x^{11} mode in the horizontal slot WG with similar WG width. The structure is not sensitive to the fluctuation of the dimension, allowing more than ± 10 nm possible fabrication tolerances in both the width and the height.

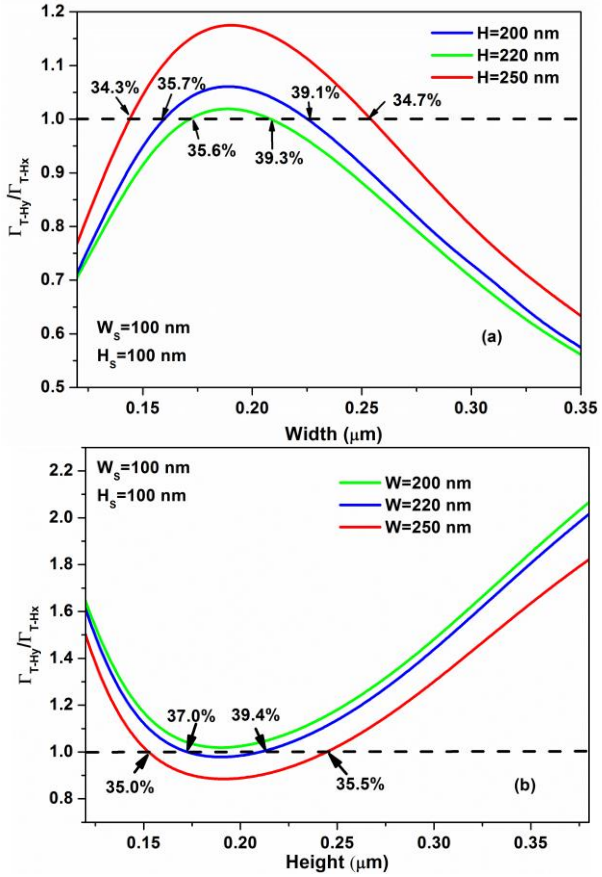

Fig. 9. Variations of $\Gamma_{T-Hy}/\Gamma_{T-Hx}$ with the (a) width, W and (b) height, H of silicon cores.

For a polarization-independent structure which can support quasi-TE and quasi-TM modes with similar performance, besides the total-slot confinement factor, ratio of the total-slot confinement factors for the H_y^{11} and H_x^{11} modes, $\Gamma_{T-Hy}/\Gamma_{T-Hx}$, should also be calculated to optimize the cross-slot dimensions. Variations of $\Gamma_{T-Hy}/\Gamma_{T-Hx}$ with the width, W and height, H of silicon cores are shown in Fig. 9 (a) and (b), respectively. The ratio of 1 is shown here by a black dashed line. It can be observed from Fig. 9 (a) that for a given height, due to the parabolic variation tendency of Γ_{T-Hy} and the monotone-increasing variation tendency of Γ_{T-Hx} with the silicon core width, all the ratios increase at first and then decrease with the increase of the silicone core width. The red curve for H=250 nm shows that the cross-slot WG can confine equal power in the whole slot region for both the polarizations, but total-slot confinement factor for each one is around 34%. On the other hand, for H=220 nm, shown by a green line, total-slot confinement factor for each polarization can reach to the same value of 39.3%, when the silicon core width is taken as 212 nm. On the other hand, for a given width, the confinement ratios decrease at first and then increase with the increase of the silicon core height, as shown in Fig. 9 (b). It is obvious that the ratio can reach 1 at several width and height combinations. To achieve a successful polarization-independent design, the sensitivities for the H_y^{11} and H_x^{11} modes should be not only nearly the same but also large enough, so the width and height of the silicon cores are optimized to be around 223 nm and 216 nm, with the total-slot confinement factor for each polarization of 39.4%. It can also be observed here that the performance would be remarkably stable even for a possible ± 10 nm fabrication error of the silicon core dimensions.

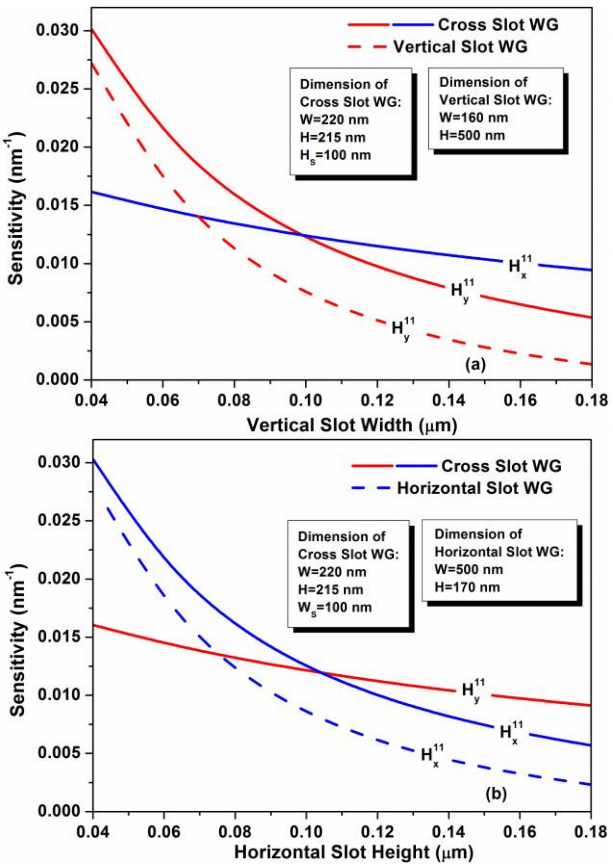

Fig. 10. Variations of sensitivities with the slot dimension for different polarizations in the vertical, horizontal, and cross-slot waveguides: (a) with the vertical slot width for the vertical and cross-slot waveguides, (b) with the horizontal slot height for the horizontal and cross-slot waveguides.

Next, the WG sensitivity, S, instead of the confinement factor in the slot region is employed to optimize the slot dimension of the cross-slot WG, because the ratio of the confinement factors in the sensing layer and slot region is no longer fixed in this case, and thus the positive correspondence relation between them is broken. The change in n_{eff}, Δn_{eff}, due to an increase in the sensing layer thickness is calculated, when this layer is completely saturated with the analyte. Here, the

sensing layer increment, $\Delta\tau$ is taken as 2.5 nm. The relation $S = \Delta n_{eff}/\Delta\tau$ is applied here to calculate the sensitivity. In order to compare the sensitivity performance of a biochemical sensor based on the vertical, horizontal, and cross-slot WGs, the sensitivities of all three types of sensors are calculated. Variations of sensitivities for the H_y^{11} and H_x^{11} modes in the cross-slot WG, and the H_y^{11} mode in vertical slot WG with the width of the vertical slot, are shown in Fig. 10 (a). The silicon core width and height, and the horizontal slot height of cross-slot WG are taken as 220 nm, 215 nm, and 100 nm, respectively. To obtain a fair comparison, the silicon core height of vertical slot WG is set to 500 nm, close to the cross-slot WG total height, and its silicon core width is set to 160 nm where the sensitivity of the vertical-slot-WG sensor with the given height reaches its peak value. It can be observed that with the decrease of the slot width, all the sensitivities increase, and sensitivity for the H_y^{11} mode either in a cross or vertical slot WG increases more quickly than that for the H_x^{11} mode in the cross-slot WG. It can also be observed that for the H_y^{11} mode, the sensitivity of the cross-slot WG is much better than that of the vertical slot WG, for instance, when the slot width is 100 nm, the values of sensitivities of the sensors based on these two WGs are 0.012 nm^{-1} and 0.007 nm^{-1}, which may be caused by larger interaction area in the slot region of the cross-slot WG. Correspondingly, variations of sensitivities for the H_x^{11} and H_y^{11} modes in the cross-slot WG, and the H_x^{11} mode in horizontal slot WG with the horizontal slot height shown in Fig. 10 (b) demonstrate similar characteristics. Overall, the sensitivities of cross-slot WG for both the H_y^{11} and H_x^{11} modes can be increased by reducing the vertical slot width and horizontal slot height. A bio-medical sensors based on the novel cross-slot WGs is expected not only to be polarization independent but also to be more sensitive than the ones based on only a vertical or horizontal slot.

To measure the effective index change of a cross-slot WG during the sensing process, this cross-slot WG can be incorporated in a Mach-Zehnder (MZ) interferometer [9]. By introducing the cross-slot WG in one arm of the MZ interferometer through the well-designed adiabatic tapers, and a reference cross-slot WG in the other arm, the relative phase shift, $\Delta\varphi$ can be obtained from the change in the effective index, Δn_{eff}, as

$$\Delta\varphi = \Delta n_{eff} \cdot \frac{2\pi}{\lambda} \cdot L \tag{5}$$

The destructive interference of signals occurs when $\Delta\varphi$ equals to π. Here, the length of the MZI arm (L) with cross slot waveguide is calculated to be 12.9 μm, when the silicon core width and height, and the slot height and width are taken as 220 nm, 215 nm, 100 nm, and 100 nm, respectively, and the thickness change of sensing layer is taken as 5 nm.

IV. Fabrication Challenges

Fabrication of the proposed cross-slot WG would be more difficult than that of a vertical slot WG, as this is a multilayer structure and also contains a hollow horizontal slot. However, we believe that such a structure can be fabricated by exploiting the well-developed CMOS technology.

The uniformity of four silicon cores on two different silicon layers would be the first challenge. In order to reduce the deviation among them, the deposition of the two silicon layers should be finished before obtaining the cores by dry etching. Our results also show that the structure is not very sensitive to the fluctuation of the dimensions, allowing more than ± 10 nm possible fabrication tolerances in both the width and height.

The second challenge is the fabrication of a hollow horizontal slot. This structure can be designed to connect via the tapered WGs, as shown in Fig. 3 (a). Since width of the two horizontal slots in between two silicon layers is smaller, by controlling the etching process carefully and accurately, all the SiO_2 there can be removed while the silica in the wider region at the two ends is removed only partially, by which two upper silicon layers are mechanically supported.

V. Conclusion

An accurate full-vectorial **H**-field based FEM is used to study the characteristics of the biochemical sensors based on the SOI vertical, horizontal, and a novel cross-slot which is composed of both vertical and horizontal slots. For the quasi-TE polarization, the slot confinement factor of the cross-slot WG is as high as that of the vertical slot WG with the same WG height. Similarly, for the quasi-TM polarization, slot confinement factor of the cross-slot WG is also as high as that of the horizontal slot WG with the same WG width. It is true that the cross-slot WG can take advantages of both the vertical and horizontal slot WGs, and support the field enhancement in the slot region for both the quasi-TE and quasi-TM polarizations and such a structure can be easily fabricated by using standard CMOS technologies.

For unpolarized operating light, the cross-slot WG is optimized to have the maximum summation of the slot confinement factors for the two polarizations, whose values are also approximately equal to the summation of the slot confinement factors of the quasi-TE mode in the vertical slot WG with the same WG height and that of the quasi-TM mode in the horizontal slot WG with the same WG width.

A polarization-independent design of the biochemical sensor is also achieved based on the cross-slot WG successfully. When the silicon core width and height are set to around 223 nm and 216 nm, respectively, the slot confinement factor for each polarization can reach 39.4%, nearly the same as that for the quasi-TE mode in the vertical slot WG with the same WG height and also that for the quasi-TM mode in the horizontal slot WG with the same WG width.

The sensitivities of the biochemical sensors based on the three types of WGs are calculated and compared, and cross-slot-WG sensor exhibits a significantly better performance. When the vertical slot width and horizontal slot height are set to 100 nm, the maximum sensitivity of a cross-slot reported here is almost double of vertical-slot-WG or horizontal-slot-WG sensors with similar dimensions.

REFERENCES

[1] M. Lipson, "Guiding, modulating and emitting light on silicon-challenges and opportunities (Invited)," *J. Lightwave Technol.*, vol. 23, no. 12, pp. 4222–4238, Dec. 2005.

[2] S. Balslev, A. M. Jorgensen, B. Bilenberg, K. B. Mogensen, D. Snakenborg, O. Geschke, J. P. Kutter, and A. Kristensen, "Lab-on-a-chip with integrated optical transducers," *Lab on a Chip*, vol. 6, pp. 213–217, Dec. 2005.

[3] F. Dell'Olio and V. M. Passaro, "Optical sensing by optimized silicon slot WGs," *Opt. Express*, vol. 15, no. 8, pp. 4977–4993, Apr. 2007.

[4] B. J. Luff, R. D. Harris, J. S. Wilkinson, R. Wilson, and D. J. Schiffrin, "Integrated-optical directional coupler biosensor," *Opt. Lett.*, vol. 21, no. 8, pp. 618–620, Apr. 1996.

[5] F. Prieto, B. Sepulveda, A. Calle, A. Llobera, C. Domynguez, A. Abad, A. Montoya, and L M Lechuga, "An integrated optical interferometric nanodevice based on silicon technology for biosensor applications," *Nanotechnology*, vol. 14, no. 8, pp. 907–912, July 2003.

[6] T. Claes, J. G. Molera, K. De Vos, E. Schacht, R. Baets, and P. Bienstman, "Label-free biosensing with a slot-WG-based ring resonator in silicon on insulator," *IEEE Photon. J.*, vol. 1, no. 3, pp. 197–204, Sep. 2009.

[7] V. R. Almeida, Q. Xu, C. A. Barrios, and M. Lipson, "Guiding and confining light in void nanostructure," *Opt. Lett.*, vol. 29, no. 11, pp. 1209–1211, June 2004.

[8] T. Dar, J. Homola, B. M. A. Rahman, and M. Rajarajan, "Label-free slot-waveguide biosensor for the detection of DNA hybridization," *Appl. Opt.*, vol. 51, no. 34, pp. 8195–8202, Dec. 2012.

[9] C. Viphavakit, M. Komodromos, C. Themistos, W. S. Mohammed, K. Kalli, and B. M. A. Rahman, "Optimization of a horizontal slot WG biosensor to detect DNA hybridization," *Appl. Opt.*, vol. 54, no. 15, pp. 4881–4888, May 2015.

[10] B. M. A. Rahman and J. B. Davies, "Finite element solution of integrated optical Waveguides," *J. Lightwave Technol.*, vol. 2, no. 5, pp. 682–688, Oct. 1984.

[11] R. Sun, P. Dong, N. N. Feng, C. Y. Hong, J. Michel, M. Lipson, and L. Kimerling, "Horizontal single and multiple slot waveguides: optical transmission at lambda = 1550 nm," *Opt. Express*, vol. 15, no. 26, pp. 17967–17972, Dec. 2007.

[12] S. Lee, S. C. Eom, J. S. Chang, C. Huh, G. Y. Sung, and J. H. Shin, "A silicon nitride microdisk resonator with a40-nm-thin horizontal air slot," *Opt. Express*, vol. 18, no. 11, pp. 11209–11215, May 2010.

[13] S. Lee, S. C. Eom, J. S. Chang, C. Huh, G. Y. Sung, and J. H. Shin, "Label-free optical biosensing using a horizontal air-slot SiNx microdisk resonator," *Opt. Express*, vol. 18, no. 20, pp. 20638–20644, Sep. 2010.

[14] J. Chee, S. Zhu, and G. Q. Lo, "CMOS compatible polarization splitter using hybrid plasmonic waveguide," *Opt. Express*, vol. 20, no. 23, pp. 25345-25355, Nov. 2012.

[15] A. Gupta, D. Akin, and R. Bashir, "Detection of bacterial cells and antibodies using surface micromachined thin silicon cantilever resonators," *J. Vac. Sci. Technol.*, B, vol. 22, no. 6, pp. 2785-2791, Nov. 2004.

[16] K. De Vos, J. Girones, S. Popelka, E. Schacht, R. Baets, and P. Bienstman, "SOI optical microring resonator with poly(ethylene glycol) polymer brush for label-free biosensor applications," *Biosens. Bioelectron.*, vol. 24, no. 8, pp. 2528-2533, Apr. 2009.

[17] C. A. Barrios, M. J. Bañuls, V. González-Pedro, K. B. Gylfason, B. Sánchez, A. Griol, A. Maquieira, H. Sohlström, M. Holgado, and R. Casquel, "Label-free optical biosensing with slot-waveguides," *Opt. Lett.*, vol. 33, no. 7, pp. 708–710, Mar. 2008.

Chao Pan received the B.Sc. Eng. Degree from the School of Electronic Science & Engineering, Southeast University, Nanjing, P. R. China in 2009. He is currently a Ph D student at Southeast University, Nanjing, P. R. China. In Nov. 2014, he was exchanged to City University, London, U.K., for 1 year mobility PhD study sponsored by INTACT program.

B. M. A. Rahman (S'80–M'83–SM'94-F'15) received the B.Sc. Eng. and M.Sc. Eng. degrees (with distinctions) in electrical engineering from Bangladesh University of Engineering and Technology (BUET), Dhaka, Bangladesh, in 1976 and 1979, respectively, and the Ph.D. degree in Electronics from University College London, London, U.K., in 1982.

From 1976 to 1979, he was a Lecturer in the Department of Electrical Engineering, BUET. In 1982, he was a Postdoctoral Research Fellow at University College London, where he continued his research on the development of finite-element method for characterizing optical guided-wave devices. In 1988, he joined City University, London, as a Lecturer, where he is now a Professor, and leads the research group on photonics modeling, specialized in the use of rigorous and full-vectorial numerical approaches to design, analyze, and optimize a wide range of photonic devices, such as spot-size converters, high-speed optical modulators, compact bend designs, power splitters, polarization splitters, polarization rotators, polarization controllers, terahertz devices, etc. He is the author or coauthor of more than 500 journal and conference papers, and his journal papers have been cited more than 3400 times.

Prof. Rahman received two gold medals for being the best undergraduate and graduate students of the university in 1976 and 1979, respectively. In 1979, he was awarded with a Commonwealth Scholarship to study for a Ph.D. degree in the U.K. He is a Fellow of Institute of Electrical and Electronic Engineers (IEEE), the Optical Society of America (OSA), and the International Society for Optics and Photonics (SPIE).